Ab Initio Molecular Dynamics of Protonated Dialanine and Comparison to Infrared Multiphoton Dissociation Experiments

ARTICLE *in* THE JOURNAL OF PHYSICAL CHEMISTRY A · AUGUST 2006

Impact Factor: 2.69 · DOI: 10.1021/jp062114o · Source: PubMed

Ab Initio Molecular Dynamics of Protonated Dialanine and Comparison to Infrared Multiphoton Dissociation Experiments

D. C. Marinica,[†] G. Grégoire,[‡] C. Desfrançois,[‡] J. P. Schermann,[‡] D. Borgis,*[,†] and M. P. Gaigeot*[,†,§]

Laboratoire Analyse et Modélisation pour la Biologie et l'Environnement, LAMBE, UMR-CNRS 8587, Université d'Evry val d'Essonne, Bât. Maupertuis, F-91025 Evry, France, and Laboratoire de Physique des Lasers, UMR CNRS 7538, Institut Galilée, Université Paris-Nord, F-93430 Villetaneuse, France

Received: April 5, 2006; In Final Form: May 22, 2006

Finite temperature Car−Parrinello molecular dynamics simulations are performed for the protonated dialanine peptide in vacuo, in relation to infrared multiphoton dissociation experiments. The simulations emphasize the flexibility of the different torsional angles at room temperature and the dynamical exchange between different conformers which were previously identified as stable at 0 K. A proton transfer occurring spontaneously at the N-terminal side is also observed and characterized. The theoretical infrared absorption spectrum is computed from the dipole time correlation function, and, in contrast to traditional static electronic structure calculations, it accounts directly for anharmonic and finite temperature effects. The comparison to the experimental infrared multiphoton dissociation spectrum turns out very good in terms of both band positions and band shapes. It does help the identification of a predominant conformer and the attribution of the different bands. The synergy shown between the experimental and theoretical approaches opens the door to the study of the vibrational properties of complex and floppy biomolecules in the gas phase at finite temperature.

1. Introduction

In the past few years, mass spectrometry has become a valuable and essential tool for the formation and characterization of peptides and proteins in the gas phase. This is partly due to the development of 'soft' ionization methods such as matrix-assisted laser desorption ionization (MALDI)[1] and electrospray ionization (ESI),[2−4] which allow a controlled formation of singly or multiply charged peptides and proteins in the gas phase. On the other hand, vibrational spectroscopy (infrared and Raman) has been recognized for a long time as an important tool for the characterization and understanding of molecular structures and dynamics. It is in particular commonly applied for the characterization of secondary structures of peptides and proteins in solution or membranes.[5−8] As an illustration, structural motifs such as helices or beta sheets can be identified by changes in positions, shapes, and intensities of linear infrared or Raman bands.[6,9,10]

Gas-phase mass spectrometry and infrared vibrational spectroscopy can be gathered in a setup which couples mass spectrometry (MS) with infrared multiphoton dissociation (IR-MPD), as devised at FELIX[11] or CLIO[12] in Europe. At CLIO, the ions either produced by MALDI or ESI are first stored and mass selected in a FT-ICR-MS device (Fourier transform ion cyclotron resonance MS). They are further submitted to IR-MPD, and the fragment ion yields are recorded as a function of the IR excitation energy. Note that as gas-phase ions are produced in much too small quantities to measure the direct absorption of IR photons, the absorption must be probed by a 'messenger method' (or 'secondary process'), namely, in these experiments, ion fragmentation. Conditions necessary for IR-MPD of gas phase molecules are fulfilled by using an infrared free electron laser (FEL). Thermalization of the produced ions is an important aspect of these experiments. Though the ions are initially produced at high internal energies, their trapping in the ICR cell during a few seconds before exposure to the IR radiation ensures their relaxation and thermalization at room temperature. This device therefore gives the IR spectroscopy of trapped gas-phase ions at room temperature, close enough to relevant physiological temperatures of biomolecules.

Using this experimental setup, investigations of structural and dynamical properties of biomimetic molecules have been recently undertaken by different groups.[13−18] In particular, some of us have presented results on the protonated alanine dipeptide Ala-Ala-H^+.[15] One goal was to give information on the protonation site of the peptide using IR signatures. Note that intramolecular proton transfer in ionized peptides has received a lot of attention recently. The majority of the studies have examined the role of the 'mobile proton' in explaining peptide fragmentation patterns observed in mass spectrometry experiments.[19−24] In particular, it is necessary to assume that the proton is not sequestered at basic sites but is free to migrate over different sites of the peptide before its fragmentation. Different experiments[19,25,26] can be performed in order to investigate the proton localization and proton transfer in peptides. Use of IR signatures is just another route to tackle the same problem.

Infrared measurements are generally complemented with theoretical calculations. These are usually done using quantum chemistry calculations where equilibrium conformations of lowest energies are calculated. In such a scheme, geometry optimizations at 0 K are performed, and vibrational analyses in the harmonic approximation are subsequently done for each equilibrium conformation. A match between experimental and calculated IR patterns obtained for the different conformers is

* Corresponding authors. E-mail: gaigeot@ccr.jussieu.fr; daniel.borgis@univ-evry.fr.

§ Permanent address: LPTMC, Université Pierre et Marie Curie-Paris6, UMR-CNRS 7600, 4 Place Jussieu, Case courrier 121, F-75052 Paris, France.

† Université d'Evry val d'Essonne.

‡ Université Paris-Nord.

10.1021/jp062114o CCC: $33.50
Published on Web 06/24/2006

generally checked in terms of positions and relative intensities of IR bands. The bottleneck of such theoretical calculations is thus the determination of all the representative equilibrium conformations of the molecule. This is a tremendous amount of work for flexible and floppy molecules. A small dipeptide already possesses several conformers (representative of those encountered in larger peptides) which are generally lying within a small energy range. As illustrative examples, we refer the reader to previous works on diglycine and dialanine peptides.[27−30] At room temperature, which is the typical temperature of peptide ions before IR absorption in IR-MPD experiments, one can thus expect conformational isomerization dynamics to take place. In other words, the peptide does possess enough internal energy to explore different zones of its potential energy surface (PES). Therefore, different isomeric conformations of the molecule can be accessible at that temperature and will most likely play a role on the peptide properties, i.e., its IR spectroscopy and mass spectrometry fragmentation.

Taking into account the dynamics of the molecule and its consequences on the measured properties can only be achieved through molecular dynamics simulations. In particular, DFT-based molecular dynamics simulations using the Car−Parrinello (CPMD) scheme[31] can be performed. The CPMD approach combines plane-wave/pseudopotential methods for the determination of the electronic structure of extended systems within the DFT generalized gradient approximation (GGA) developed for treating molecules. A special feature distinguishing the CPMD method from other ab initio MD methods is the dynamical scheme adopted for the optimization of the electronic states which is based on a fictitious (classical) dynamics of the electronic degrees of freedom (for a technical introduction to CPMD techniques see ref 32). The electronic degrees of freedom are therefore propagated simultaneously to the nuclear degrees of freedom. Based on first principles, CPMD simulations are hence capable of accounting for the many-body interactions and treat in a natural way bond breaking/making such as proton transfers.

In previous works, we have shown that DFT-based Car−Parrinello molecular dynamics simulations yield very accurate infrared spectra of biomimetic molecules in the gas phase or immersed in aqueous solvent at room temperature in terms of band positions, band shapes, and band intensities.[33,34] The present investigation of the gas-phase protonated Ala-Ala-H^+ peptide is aimed at demonstrating that CPMD simulations are the proper tool to calculate IR absorption spectra of gas-phase molecules undergoing multiple isomeric conformations at room temperature. We want to show that these simulations provide more information than 0 K geometry optimizations for the determination of IR spectra and comparison to experiments. Moreover, as we will see below, CPMD simulations give us the opportunity to follow the dynamics of the excess proton which is of special interest for the protonated Ala-Ala-H^+ peptide ion investigated here.

The paper is organized as follows. The CPMD method as well as the way infrared spectra are extracted from the dynamics is presented briefly in section 2. Section 3.1 presents our findings on the conformational dynamics of Ala-Ala-H^+ at room temperature and especially emphasizes the transfer dynamics of the excess proton. Section 3.2 reports our calculated infrared absorption spectrum of Ala-Ala-H^+ at room temperature and its interpretation in terms of intramolecular motions. Comparison is made with IR-MPD spectra. Discussion and perspectives are finally presented in section 4.

2. Computational Method

The DFT-based Car−Parrinello simulations performed in this work follow the general setup of our previous ab initio molecular dynamics simulations.[33−35] We used the Becke, Lee, Yang, and Parr (BLYP) gradient-corrected functional[36,37] for the exchange and correlation terms. The one-electron orbitals are expanded in a plane-wave basis set with a kinetic energy cutoff of 70 Ry restricted to the Γ point of the Brillouin zone. Medium soft norm-conserving pseudopotentials of the Martins−Trouillier type[38] are used. The core-valence interaction of C, N, and O is treated by *s* and *p* potentials with pseudization radii of 1.23, 1.12, and 1.05 au, respectively (taking the same radius for *s* and *p*), while H atoms are treated as an *s* potential with a 0.5 au radius. Energy expectations are calculated in reciprocal space using the Kleinman−Bylander transformation.[39]

The value of 70 Ry for the energy cutoff of the plane wave expansion of the wave function has been checked with the following scheme. We have taken the geometries of the four conformers of least energy of Ala-Ala-H^+ optimized at the DFT/B3LYP/6-31G* level of calculation by Lucas et al.[15] and reoptimized them at the DFT/BLYP/6-31G* level with the Gaussian98 package.[40] The four optimized geometries are schematically represented in Figure 1 where the adopted nomenclature is also reported (namely transA1, transA2, transO1, and cisA3). The trans/cis nomenclature corresponds to the isomerization state of the NH−CO internal peptide bond in the dipeptide. TransA1/A2 are connected to each other by mere rotation around the $N-C_3$ bond. TransO1 is obtained from transA1 by transferring a proton from the terminal NH_3^+ to the adjacent C═O bond. TransA1 is the conformer of least energy, while transO1, transA2, and cisA3 appear at the BLYP level with higher energies of +1.76, +2.15, and +2.45 kcal/mol, respectively (these energies include the zero point vibrational energy correction, as in ref 15). We have subsequently made single point electronic calculations on the BLYP optimized conformations using the plane-waves CPMD code, with two different energy cutoff values for the plane wave expansion, 70 and 140 Ry. We have compared the energetical order and the energy difference for the four conformations. Both plane-wave calculations give the same energetical order, i.e., transA1, transA2, transO1, cisA3, with the following energy gaps with respect to transA1 (values from the 140 Ry cutoff reported in parentheses): +1.83(+1.75), +2.13(+2.03), +3.21(+2.99), in kcal/mol. There is thus a very slight and meaningless 0.1−0.3 kcal/mol decrease in energy when going from a 70 to a 140 Ry cutoff. Using a cutoff of 70 Ry appears therefore sufficient to treat the interactions in Ala-Ala-H^+ peptide. The plane-wave BLYP single point calculations give an inversion between transO1 and transA2 energies in comparison to the BLYP/6-31G* optimizations.

Car−Parrinello molecular dynamics simulations were performed at constant volume (microcanonical ensemble) using a fictitious electron mass of 500 au and a time step of 5 au (0.12 fs). The Car−Parrinello technique is based on the use of an extended Lagrangian for the description of the coupled motion of nuclei and electrons, where a fictitious electronic mass is assigned to the electronic degrees of freedom. The chosen value of 500 au provides a correct separation of time scales between the nuclei and fictitious electron dynamics. Gas-phase simulations were carried out with the decoupling technique of Martyna and Tuckerman[41] in order to eliminate the effect of the periodic images of the charge density. A cubic box of length 20 Å was selected after performing a series of wave function optimizations of Ala-Ala-H^+ conformers in boxes of increasing length. We found that from 20 Å on, the electronic energy of the isolated

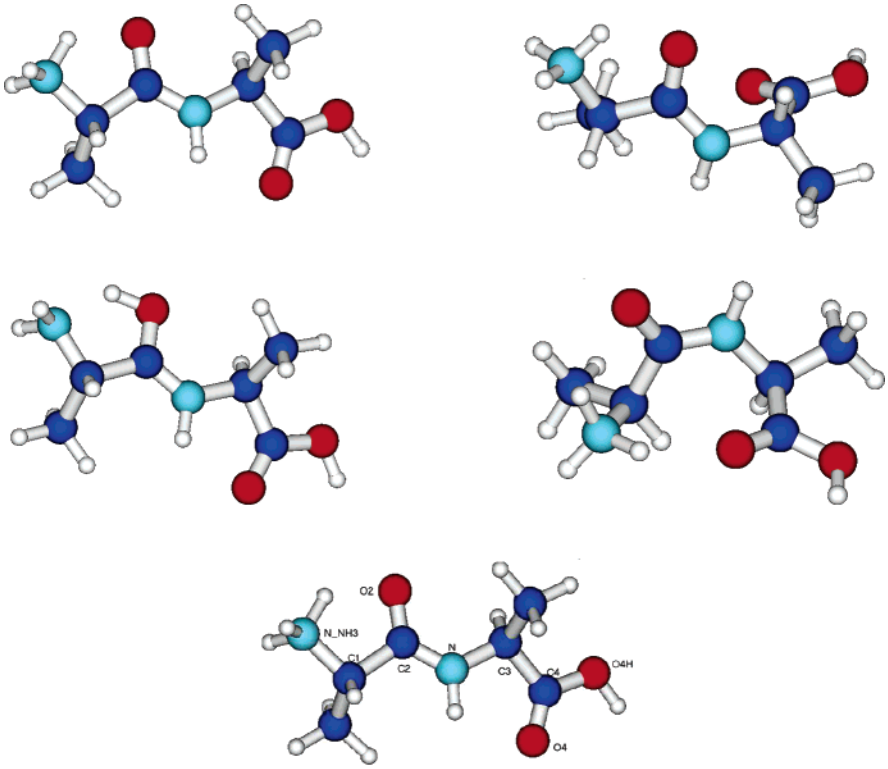

Figure 1. Schematic representation of the four main structures of lower energy of gas-phase Ala-Ala-H$^+$ peptide optimized in ref 15 and in this work: top, transA1 (left) and transA2 (right) and bottom, transO1 (left) and cisA3 (right). The lower part of the figure displays the atom numbering adopted in this work. Carbon atoms are represented in dark blue, nitrogen atoms in light blue, oxygen atoms in red, and hydrogen atoms in gray.

molecule is converged within a criterion of 10^{-4} au, which ensures that the wave function of the isolated molecule is all contained in the cell box. Car−Parrinello molecular dynamics simulations reported here consist of two steps: an equilibration phase of 1−3 ps with a control of temperature through velocity rescaling, followed by data collection over trajectories of either 3.5 or 7.0 ps. In that step, molecular dynamics are strictly microcanonical. We have performed nine different Car−Parrinello molecular dynamics simulations, from which eight simulations were begun from trans Ala-Ala-H$^+$ conformations (transA1, transA2, or transO1) and one from cisA3 Ala-Ala-H$^+$ conformation. Initial velocities were chosen in a Boltzmann distribution centered at 300 K. The average ionic temperature obtained over all simulations was 279 ± 13 K. Equipartition of energy over all degrees of freedom is globally respected as we obtained the following averaged temperatures per atomic type: 270 ± 6 K for nitrogen atoms, 270 ± 11 K for hydrogen atoms, 280 ± 17 K for carbon atoms, and 296 ± 17 K for oxygen atoms. Hydrogen atoms were treated as classical particles with their true mass (1836 au). All simulations were carried out with version 3.7 of the CPMD ab initio molecular dynamics package.[42] Since the simulations are performed in the microcanonical ensemble, and molecular vibrational energy transfers are rather slow, performing several short-time independent dynamics starting from canonical velocities instead of a single long trajectory improves the phase space sampling.

The calculation of the infrared (IR) absorption coefficient $\alpha(\omega)$ makes use of a relation (derived from linear response theory) involving the Fourier transform of the dipole time correlation function or equivalently its time derivative (current) $\dot{\mathbf{M}} = d\mathbf{M}/dt$ with[43]

$$\alpha(\omega)n(\omega) = \frac{2\pi\beta}{3cV}\int_{-\infty}^{+\infty}\langle\dot{\mathbf{M}}(0)\dot{\mathbf{M}}(t)\rangle e^{i\omega t}dt \qquad (1)$$

where $\beta = 1/k_BT$, $n(\omega)$ is the refractive index, c is the speed of light in vacuum, and V is the volume. The angular brackets in formula (1) indicate a statistical average over all the generated trajectories. Note that in this formula we have taken into account a quantum correction factor (multiplying the classical line shape) of the form $\beta\hbar\omega/(1 - \exp(-\beta\hbar\omega))$, which was shown to give the most accurate results for IR intensities.[33,34,44] For a complete discussion on quantum corrections, we refer the reader to refs 45 and 46. The IR spectrum is defined as the product $\alpha(\omega)$-$n(\omega)$, ω in cm^{-1}. Derivatives $d\mathbf{M}/dt$ have been calculated numerically. $\mathbf{M}$ is the total dipole moment of the system, which is the sum of the ionic and electronic contribution. The dipole moment of the box cell is calculated with the Berry phase representation, as implemented in the Car−Parrinello framework.[47−49] Briefly, in the limit where the Γ point approximation applies, the electronic contribution to the cell dipole moment $\mathbf{M}_\alpha^{el}$ (where $\alpha = x, y, z$) is given by[50]

$$\mathbf{M}_\alpha^{el} = \frac{e}{|\mathbf{G}_\alpha|} Im\ \mathrm{ln}z_N \qquad (2)$$

where $Im\ \mathrm{ln}z_N$ is the imaginary part of the logarithm of the dimensionless complex number $z_N = \langle\Psi|e^{-i\mathbf{G}_\alpha\cdot\hat{\mathbf{R}}}|\Psi\rangle$, $\mathbf{G}_\alpha$ is a reciprocal lattice vector of the simple cubic supercell of length L ($\mathbf{G}_1 = 2\pi/L(1,0,0)$, $\mathbf{G}_2 = 2\pi/L(0,1,0)$, $\mathbf{G}_3 = 2\pi/L(0,0,1)$), and $\hat{\mathbf{R}} = \sum_{i=1}^{N}\hat{\mathbf{r}}_i$ denotes the collective position operator of the N electrons (or in other words the center of the electronic charge distribution). Ψ is the ground-state wave function. The quantity Im $\mathrm{ln}z_N$ is the Berry phase, which in terms of a set of occupied Kohn−Sham orbitals $\psi_k(\mathbf{r})$ is computed as Im $\mathrm{ln}z_N = 2Im\ \mathrm{ln}det\mathbf{S}$ with elements of the matrix $\mathbf{S}$ given by $S_{kl} = \langle\psi_k|\ e^{-i\mathbf{G}_\alpha\cdot\hat{\mathbf{r}}}|\psi_l\rangle$.[50]

The final spectra presented in section 3.2 was obtained by Fourier transform of an averaged correlation function computed from all trajectories corresponding to a given conformer (cis or trans). A final smoothing of the spectrum was achieved through

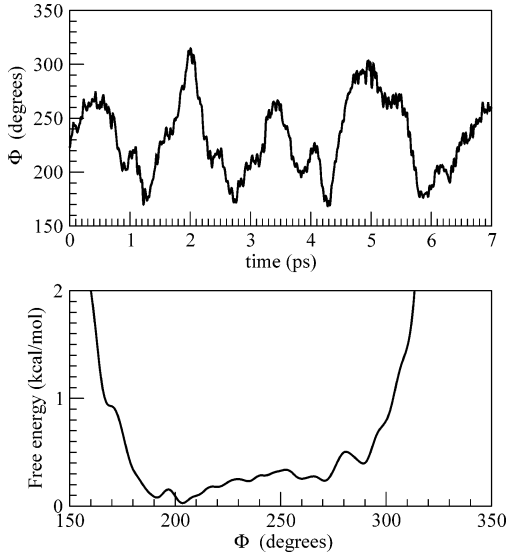

Figure 2. Top: Time evolution of the dihedral angle $\Phi = C_2-N-C_3-C_4$ for a typical CPMD trajectory of the trans isomer at 300 K. See Figure 1 for atomic labeling. Time in picoseconds and angles in degrees. Bottom: Free energy profile along the Φ dihedral angle averaged over all trans trajectories. See text for explanations.

a window filtering applied in the time domain which corresponds roughly to the convolution of the bare spectrum by a 8 cm^{-1} width Gaussian function. This is comparable to the apparatus function inferred for IR-MPD spectra.[15]

3. Results

3.1. Conformational Dynamics of Ala-Ala-H$^+$ at 300 K. *A. Isomerization Dynamics between transA1 and transA2.* All trajectories concerning trans type conformations of Ala-Ala-H$^+$ showed a continuous isomerization dynamics between transA1 and transA2 conformers (except for a short 3-ps trajectory where the dynamics remained confined in the transA1 basin). This can be appreciated by following the time evolution of the dihedral angle $\Phi = C_2-N-C_3-C_4$ (see Figure 1 for atom labeling): the value of this angle is indeed a signature distinguishing a geometry typical of transA1 (Φ=198.1°) versus transA2 (Φ=284.2°) in reference to our BLYP/6-31G* 0 K geometry optimizations. Note that we express here all angles in the 0−360° range, which was not the convention taken in ref 15. Figure 2a illustrates this conformational isomerization dynamics for one typical CPMD trajectory at 300 K. The continuous evolution of Φ between roughly 180° and 300° reveals the exploration of the two basins associated to transA1 and transA2 on the potential energy surface (PES) at room temperature. In other words, the internal energy of the peptide at 300 K is sufficient to overcome the energy barrier separating the transA1 and transA2 basins on the PES. This observation can be substantiated by plotting the free-energy curve, $G(\Phi) = -k_BT \ln(P(\phi))$, where $P(\phi)$ is the probability of occurrence of a certain angle ϕ in the course of the dynamics; see Figure 2b. The free energy curve presents a primary minimum corresponding to the transA1 conformation around 200° and a shallow metastable secondary minimum around 270° associated to transA2. It is not clear if the superimposed little wiggles, e.g. at 195 and 280°, have any statistical relevance. It is noteworthy however that the potential is going uphill rather smoothly from transA1 to transA2, with no evident barrier, and yielding an overall free energy difference of 0.3 kcal/mol between the two structures. This value is quite far from the 2 kcal/mol energy difference between the two conformers and from the ∼2.5 kcal/mol (at the B3LYP level[15]) energy difference between transA1 and the transA1-transA2 transition state, computed at 0 K. These findings clearly illustrate the importance of entropic contributions in structural equilibria.

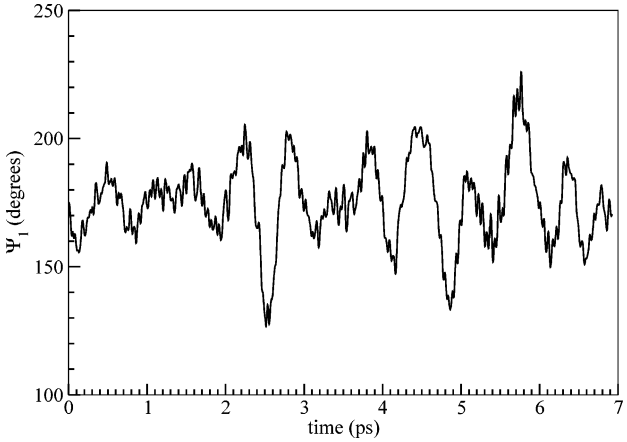

Figure 3. Time evolution of the dihedral angle $\Psi_1 = N_{NH3}-C_1-C_2-N$ for a typical CPMD trajectory of the trans isomer at 300 K. See Figure 1 for the atom labeling. Time in picoseconds, angles in degrees.

TABLE 1: Structural and Energetic Characteristics of the Four Main Structures of Lower Energy of Gas-Phase Ala-Ala-H$^+$ Peptide Optimized at the DFT/BLYP/6-31G* Level of Calculation in This Work[a]

conformer	Ψ_1	ω	Φ	Ψ_2	ΔE^b	ΔE^c	ΔE^d
transA1	176.2	177.2	198.1	173.1	0.00	0.00(0.00)	0.00
trans O1	179.4	179.2	195.6	172.8	+1.76	+2.13(2.03)	+1.73
transA2	167.1	162.2	284.2	177.8	+2.15	+1.83(1.75)	+1.73
cisA3	127.2	333.9	304.4	209.7	+2.45	+3.21(2.99)	+1.63

[a] Definition of angles (see Figure 1): $\Psi_1 = N_{NH3}-C_1-C_2-N$, $\omega = C_1-C_2-N-C_3$, $\Phi = C_2-N-C_3-C_4$, and $\Psi_2 = N-C_3-C_4-O_{4H}$. [b] Relative energies in kcal/mol obtained from geometry optimizations at the DFT/BLYP/6-31G* level of calculation done in this work. Energies include ZPE corrections. [c] Relative energies in kcal/mol obtained from single point calculations at the DFT/BLYP level using a 70 Ryd energy cutoff plane-waves basis set and Martins-Trouillier pseudopotentials. In parentheses, energies obtained with a 140 Ryd energy cutoff. [d] Relative energies in kcal/mol obtained from geometry optimizations at the DFT/B3LYP/6-31G* level of calculation from ref 15. Energies include ZPE corrections.

Meanwhile, as illustrated in Figure 3 for a typical trajectory, the dihedral angle $\Psi_1 = N_{NH3}-C_1-C_2-N$ (see Figure 1 for the atom labeling) roughly evolves between 130° and 220°, with an average value of 175 ± 16°. This reveals dynamical deformations of ∼50−60° from optimized trans geometries, where Ψ_1 = 165−180° depending on the trans conformation (see Table 1). This reflects more or less the amplitude of the NH_3^+ group rotation with respect to the C_1-C_2-N peptide backbone. In particular, the NH_3^+ group oscillates from one side of the C_1-C_2-N plane ($\Psi_1 \leq 180°$) to the other side ($\Psi_1 \geq 180°$). The NH_3^+ rotation is accompanied by the adjacent methyl group rotation, also attached to the backbone C_1 atom. Along the same lines, the dihedral angle $\Psi_2 = N-C_3-C_4-O_{4H}$ roughly evolves from 120° to 230° along the trajectories, with an average value of 168 ± 19° (curve not displayed). Again, this corresponds to an internal rotation of the hydroxyl OH group back and forth away from the $N-C_3-C_4$ plane with an amplitude up to ∼40−50°. Note also that there is no hydrogen bond between O_4 and the H atoms of the carboxylic C-terminal group of the peptide, as they are always found 2.2−2.3 Å apart from each other in all trajectories.

The trajectory obtained for a cis type peptide (curve not displayed) shows that Ψ_1 evolves between 110° and 200°; we

even observed an angle of ~50° during a very short period of time (200 fs). On average, $\Psi_1 = 149° \pm 29°$. The dynamics therefore involves strong deformations from the 127° obtained for the cisA3 optimized geometry. In the same spirit, Ψ_2-fluctuations show that the C-terminal part of the cis peptide undergoes strong deformations at 300 K. Overall, N- and C-terminal parts of the Ala-Ala-H^+ peptide seem equivalently free to rotate around the peptide backbone in trans and cis conformations.

On the other hand, deformation of the backbone structure can be followed through the time evolution of the dihedral angle $\omega = C_1-C_2-N-C_3$. This angle evolves between 150° and 220° for the trans conformations (average of ~176° ± 11) and between −60° and +40° (average of ~ −13.0° ± 22.0) for the cis ones. Comparison with the optimized geometry values (Table 1) shows that the dipeptide backbone undergoes small but finite deformations, of the order of 10−20°.

As expected, we did not observe any isomerization between the trans and cis conformers in our simulations. The cis/trans peptide bond isomerization barrier is generally estimated as a few tens of kcal/mol.[52,53] The transA1 to cisA3 peptide bond isomerization barrier has been calculated at 24 kcal/mol[15] (B3LYP level of theory). It is much too high to be observed spontaneously at room temperature.

B. Proton Transfers along the Dynamics. We address here the fundamental question of the location and dynamics of the excess proton of the ionized Ala-Ala-H^+ dipeptide. Is this proton always located on the N-terminal side of the dipeptide, thus giving rise to a NH_3^+ terminal group, or can it be located on other sites thus leaving a NH_2 group? For Ala-Ala-H^+, the only other energetically favorable protonation site is the $C_2=O_2$ carbonyl group located at the N-terminal side. Quantum calculations done in ref 15 and here do identify a hydrogen bond between $C_2=O_2$ and one hydrogen atom attached to NH_3^+ in the optimized transA conformations. The question of localization and dynamics of the excess proton is a fundamental question to address, particularly in the context of the 'mobile proton' model, evoked for certain fragmentation patterns observed in mass spectrometry experiments.[19−24] These experiments can only be interpreted by assuming that the proton is not sequestered at basic sites but is free to migrate over different sites of the peptide before fragmentation. We here investigate such a dynamics using our Car−Parrinello molecular dynamics approach. To that end, we study the time evolution of $O_2\cdots H$ distances where H is one of the three hydrogen atoms of the terminal NH_3^+ group.

Proton motions are illustrated in Figure 4 for two selected trajectories. For further comparisons, we recall the bond lengths pertinent to the optimized geometries of the three isomers of trans Ala-Ala-H^+: $O_2\cdots H = 1.70$ Å and $N-H = 1.07$ Å for transA1, $O_2\cdots H = 1.75$ Å and $N-H = 1.06$ Å for transA2, and $O_2-H = 1.04$ Å for transO1.

Indeed, it appears that transA1/A2 are more stable structures than transO1. Most of the time, the excess proton remains located on NH_3^+. At times however, a proton transfer to $C_2-O_2-H^+$ occurs. Three such events were recorded over the eight monitored trans trajectories. Two of them can be distinguished on the same trajectory on Figure 4a, one for 600 fs, and a subsequent one for 100 fs. This indicates that transO1 is a metastable state which is thermally accessible at 300 K. Indeed, when the trajectory was initiated from transO1, a rapid conversion to transA1 could be observed. The proton-transfer free energy curve $G(d_{O_2H}) = -k_BT\ln(P(d_{O_2H}))$ is displayed in Figure 5; d_{O_2H} is the distance of the O_2 to the closest proton (there can be interchanges, see below), and $P(d_{O_2H})$ is the associated probability histogram. Clearly, a sharp metastable well corresponding to the $O-H^+$ form is present. The ratio of thermal population of the two wells yields an overall free-energy difference of 2 kcal/mol (to be compared with the ~2 kcal/mol difference between the well minima). Note that inclusion of nuclear quantum effects, yielding a zero-point-energy of 3−4 kcal/mol for a proton in O−H bonds, might well wipe the metastable well out.

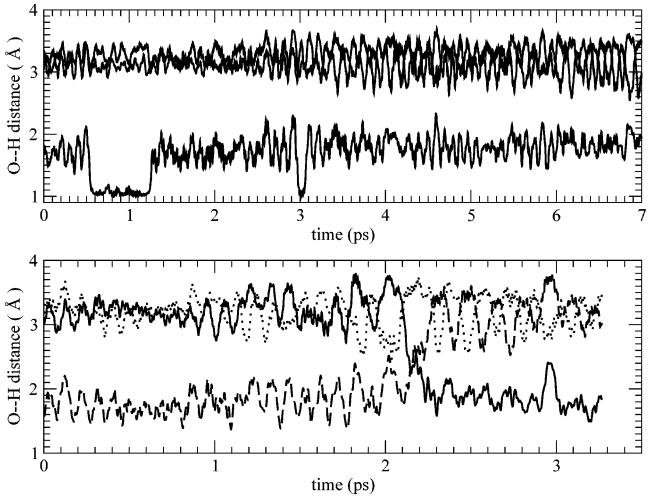

Figure 4. Time evolution of the $O_2\cdots H$ distances for two different trajectories. In the first one (top) two proton-transfer events yielding the transO1 isomer are detected, whereas in the second trajectory (bottom) the proton of NH_3^+ H-bonded to O_2 is interchanged by hindered rotation (see solid and dashed lines). See the text for details.

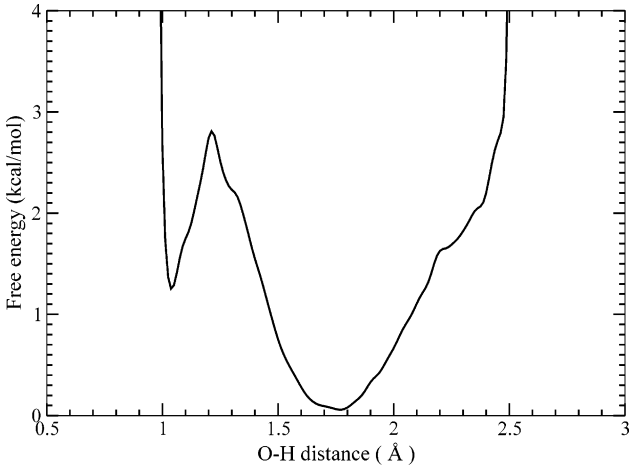

Figure 5. Free-energy profile along the $O_2\cdots H$ distance averaged over all trans trajectories.

Figure 4b illustrates a nonreactive isomerization in A-form in which the proton involved in the $H\cdots O_2$ bond is interchanged, i.e., a thermally activated rotation of the NH_3^+ group occurs. A single successful event of this sort was recorded, meaning that the interchange barrier is rather high with respect to k_BT.

Last to mention, no proton transfer was observed along the 7 ps long trajectory generated for cisA3.

3.2. Infrared Spectroscopy and Comparison to IRMPD Experiments. *3.2.1. Dipole Moments.* The time evolution of the norm of the dipole moment of Ala-Ala-H^+ obtained along three typical Car−Parrinello molecular dynamics simulations is presented in Figure 6. For comparison, we recall the values calculated for the four optimized geometries at the BLYP level

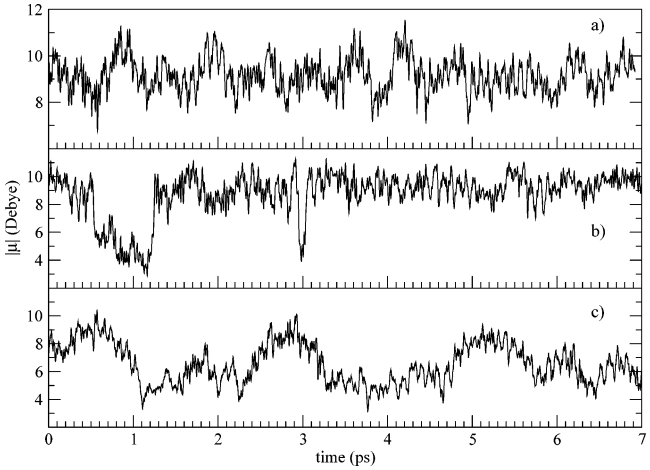

Figure 6. Time evolution of the dipole norm of Ala-Ala-H$^+$ extracted from three CPMD trajectories at 300 K corresponding to (a) the trans isomer with transA1-transA2 conformational dynamics, (b) the trans isomer with two proton-transfer events from NH_3^+ to H^+-O_2, and (c) the cis isomer. Dipoles are in Debye, time in picoseconds.

(plane-wave calculation): 8.9 D for transA1, 8.8 D for transA2, 4.9 D for transO1, and 4.9 D for cisA3. Thus the transA1 and transA2 isomers cannot be distinguished through their dipole norm. On the contrary, transO1 has a dipole which is half that of transA conformers. The dynamics presented in Figure 6a again illustrates the conformational dynamics between transA1 and transA2. The dipole norm oscillates between 6.7 and 11.5 D, with an average value of 9.2 D. The average value is characteristic of transA isomers, whereas the fluctuation amplitude of about 2 D nicely illustrates the conformational flexibility between the two forms. Figure 6b concerns the same trajectory as Figure 4a, and proton-transfer events between NH_3^+ and $C_2{=}O_2$ are easily recognizable at times ∼1 and 3 ps. When the proton has transferred from NH_3^+ to $C_2{=}O_2$, the dipole decreases to values around 4−5 D. Otherwise, the dipole norm oscillates between ∼6 and ∼12 D as typical for the transA form. Dynamical outputs for the cis conformer are presented in Figure 6c. Evidently very large oscillations of the dipole take place, with values between 3.1 and 10.4 D yielding an average value of 6.5 D. Low dipole values of ∼4−5 D typical of the cisA3 optimized geometry are only observed for transient periods of time (see for instance times between 1 and 2 ps or 3.2−4.8 ps). The majority of the time, distorted cis geometries with much higher dipole moments are generated. This is again a nice illustration of the conformational changes that can occur at room temperature.

3.2.2. Infrared Spectroscopy. The calculated infrared spectra of gas-phase Ala-Ala-H$^+$ in cis and trans forms are presented in Figures7 and 8. Our calculations are superimposed with the IR-MPD experiment taken from ref 15. Note immediately that more statistics have been collected for the trans isomers for reasons which will appear clear below. As the experimental spectrum has been recorded in the 1000−2000 cm^{-1} wavenumber domain, the calculated spectrum is displayed in the same domain. Since the BLYP DFT functional is known to systematically underestimate experimental frequencies, a conventional practice is to apply a constant correction factor to the theoretical results. We have adjusted exactly the position of the theoretical trans band at 1010 cm^{-1} to the band located at ∼1130 cm^{-1} in the experiment and have applied the corresponding 120 cm^{-1} blue shift to the whole spectrum. This single shift factor gave a complete alignment of the calculated infrared spectrum with respect to the experimental one in the 1000−2000 cm^{-1} spectral

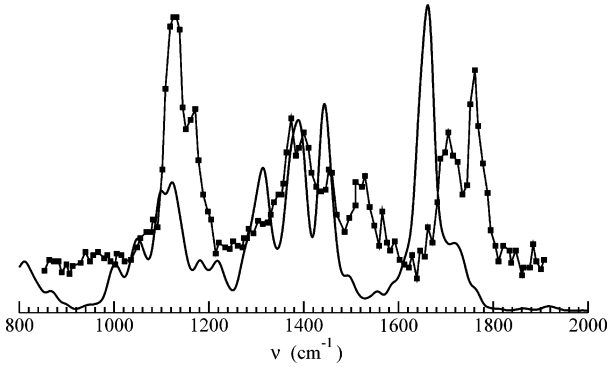

Figure 7. Infrared spectrum of gas-phase Ala-Ala-H$^+$ in cis form: squares, IR-MPD experiment taken from ref 15 and solid curve, calculation from Car−Parrinello molecular dynamics at ∼300 K.

domain. Note that this blue-shift value is very close to the one used in our previous calculations on gas-phase NMA (*N*-methylacetamide).[34] Furthermore, for easier comparison, the intensities of the theoretical spectra have been normalized so as to reproduce the absolute intensity of the 1130 cm^{-1} IR-MPD experimental band.

It appears immediately from the comparison of the cis spectrum to the experimental IR-MPD one that the experimental band located between 1500 and 1600 cm^{-1} has no theoretical counterpart. On the other hand, all bands seem to match for trans conformers. As in ref 15, it can therefore be concluded that the experimental signal is mainly due to trans conformers. This is clearly compatible with the fact that the cis optimized conformation is found 2−3 kcal/mol higher in energy than the trans one (although, as illustrated earlier for transA1/A2, this is not equivalent to a free-energy difference). Notwithstanding, we have supposed that the main contributing isomer is the trans form, and sufficient statistics have been collected for that isomer.

Interpretation of the calculated infrared active bands into individual atomic displacements is realized using the vibrational density of states (VDOS) of the peptide. The VDOS is obtained by Fourier transformation of the atomic velocity autocorrelation functions

$$\mathrm{VDOS}(\omega) = \sum_{i=1,N} \int_{-\infty}^{\infty} \mathrm{d}t \, \langle \boldsymbol{v}_{\mathbf{i}}(t) \cdot \boldsymbol{v}_{\mathbf{i}}(0) \rangle \exp(i\omega t) \qquad (3)$$

where *i* runs over all atoms of the system. In addition, we have decomposed the VDOS according to each atom type in order to get an interpretation of the vibrational bands in terms of individual atomic motions. This is done by restraining the sum over *i* in eq 3 to the atoms of interest only. This decomposition technique follows the general setup used in our previous publications.[33,34] Regarding the 1000−2000 cm^{-1} frequency domain which is of particular interest in experiments on peptides and proteins, and specifically related to the amide stretching and bending modes used for the characterization of helices and sheets structures, this simple decomposition proves sufficient to properly assign each vibrational peak of Ala-Ala-H$^+$ to specific atomic motions. The overall spectrum in the 1000−2000 cm^{-1} region can be discussed in terms of coupled stretching (ν) and bending (δ) motions, more specifically ν(C=O) (amide I) and δ(N−H) (amide II) for the peptide linkage, ν(C−C) and ν(C−N) for the peptide backbone, $\delta(NH_3^+)$ for the N-terminal region of the peptide, and δ(C=O) and δ(C−O−H) for the C-terminal region. In the present work, VDOS and its decomposition in terms of individual atomic contributions have been calculated on each trajectory, and the results have been subsequently averaged over all trajectories, again reflecting

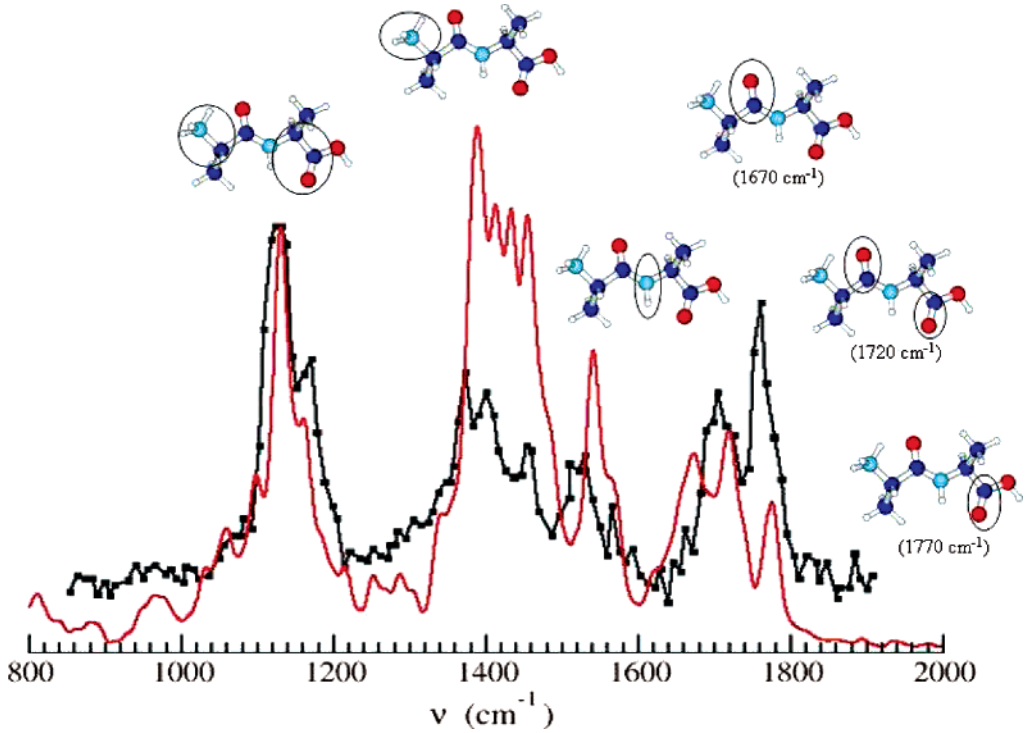

Figure 8. Infrared spectrum of gas-phase Ala-Ala-H^+ in trans form: squares, IR-MPD experiment taken from ref 15 and solid curve, calculation from Car−Parrinello molecular dynamics at ∼300 K. The band assignment deduced from the vibrational density of state (VDOS) analysis is illustrated on top.

the conformational diversity and dynamics at 300 K. The resulting band assignment for the trans isomer is represented schematically on top of the computed absorption spectrum in Figure 8 and can be commented as follows.

Both experiment and calculation display three separate absorption domains. The first domain is composed of two peaks located at 1130 and 1150 cm^{-1} which are related to stretching and bending movements of the N- and C-terminal parts of the peptide. Namely, the VDOS decomposition shows that these bands mainly correspond to a superposition of $\nu(N_{NH_3^+} - C_1)$, $\nu(C_3-C_4)$, $\delta(C_4=O_4)$, and $\delta(C_4-O_4-H)$ motions. The second infrared active domain is roughly located between 1300 and 1600 cm^{-1} and can be divided into two subdomains. The rather large band between 1340 and 1500 cm^{-1} corresponds to vibrations on the N-terminal side of the peptide, namely δ(N−H) bending motions of the NH_3^+ group coupled with skeletal ν(C−C) stretchings. The narrow band extending between 1500 and 1600 cm^{-1} is composed of the δ(N−H) amide II motion coupled with $\nu(N-C_2)$ stretching of the backbone. The final infrared active domain extends roughly between 1620 and 1800 cm^{-1} and is composed of three separate peaks in our calculation (two distinct peaks in the experiment). The peak located at 1670 cm^{-1} comes from the amide I movement of the $C_2=O_2$ carbonyl group. The peak at 1720 cm^{-1} is related to a superposition of the two amide I motions, i.e., $\nu(C_2=O_2)$ and $\nu(C_4=O_4)$ stretchings, whereas the peak at 1770 cm^{-1} involves the $C_4=O_4$ carbonyl group only.

As stated at the beginning of the discussion with the comparison of Figures 7 and 8, the 1500−1800 cm^{-1} features clearly allow discrimination between trans and cis conformers. In fact, in this domain, the trans IR spectrum displays two bands related to the carbonyl stretches (1600−1800 cm^{-1}) and one band related to the amide N−H bending (∼1500 cm^{-1}), while the cis IR spectrum is composed of only one band roughly located between these two bands. Most remarkably, interpretation of this band shows the coupling of $\nu(C_2=O_2)$ and δ(N−H) of the cis peptide bond, which was not present in the case of trans conformers. $\nu(C_2=O_2)$ and δ(N−H) movements therefore merge in one common active IR band when the peptide bond of the dipeptide adopts a cis orientation.

In Figure 8 we compare the theoretical IR absorption spectrum of protonated trans dialanine, computed according to eq 1, to the IR multiphoton dissociation spectrum obtained in a previous work.[15] Note immediately that, although they do reflect the same underlying vibrational properties, stationary IR absorption and IR-MPD experiments are by no means equivalent. The former measures the Fourier transform of the equilibrium dipole time correlations (eq 1), whereas the latter provides a nonequilibrium ionic dissociation yield as a function of IR excitation frequency. We think however that comparing band positions and band shapes makes sense, and this assertion is substantiated by the results below. Regarding intensities, although it is commonly believed that in IR-MPD the relative intensities are governed by the absorption of the few first photons, the direct comparison is much more subject to caution. That stated, the agreement between calculations and experiments appears quite satisfactory. This is revealed by the three separate IR active domains which are reproduced with a very good accuracy by the calculations, in terms of both band relative positions and bandwidths. The relative positions of the different bands as well as fine details such as the two sub-bands of the 1100−1200 cm^{-1} domain or the two distinct IR active bands of the 1300−1600 cm^{-1} domain are very well reproduced too. The amide I domain is clearly composed of three bands of high intensity in our calculation, while the experiment offers only two such bands, although a third subpeak of far lower intensity may be distinguished in the 1660 cm^{-1} tail of this domain. Overall, the theoretical band shapes and bandwidths are in satisfactory agreement with the ones experimentally observed. Considering band intensities, and keeping the above restrictions in mind, we remark the relative intensities of the sub-bands in either the 1000−1200 cm^{-1} or 1300−1600 cm^{-1} domain are well

respected with respect to the experimental ones, although the relative intensity of the two domains is clearly different. The same consideration is not at all clear in the 1600−1800 cm^{-1} due to the presence of three sub-bands instead of two.

It is important to stress again here that the only manipulation allowed for the theoretical spectrum in Figure 8 was the convolution by a 8 cm^{-1} Gaussian (comparable to the experimental apparatus function) smoothing a bit the bare results. All pertinent band shaping effects, such as anharmonicity and temperature, were incorporated ab initio via the CPMD methodology. This is to be contrasted with traditional theoretical calculations in which a normal mode spectrum for different frozen structures is convoluted by an arbitrary Lorentzian function to best fit the experimental bandwidths and accommodate a posteriori for temperature and anharmonic effects.

4. Conclusions and Perspectives

We have presented DFT-based Car−Parrinello molecular dynamics simulations at 300 K of the gas-phase ionized Ala-Ala-H^+ peptide, in both trans and cis form, in relation to a previous IR-MPD experimental study. For the trans structure, which is the energetically favored one, our simulations showed a continual and repeated isomerization dynamics between two conformers, transA1 and transA2. One important result is the observation of spontaneous proton-transfer events between NH_3^+ and the adjacent C═O group at the N-terminal side of the peptide. Overall, the simulations showed that the peptide is on average preferentially protonated at its N-terminal side yielding NH_3^+, but H^+−O−C is a thermally accessible metastable state. The infrared absorption spectrum of Ala-Ala-H^+ has been computed by average on all available trans trajectories. This average allowed to account correctly for the influence of the conformational dynamics of the peptide at 300 K on the infrared properties. We found an excellent agreement with the experimental IR-MPD spectrum in terms of band positions, band shapes, and bandwidths. This agreement is superior to that obtained previously with static ab initio calculations. The success of our dynamic approach can be explained by the following arguments.

(i) Room-temperature dynamics showed a continual conformational dynamics between the two major isomers named transA1 and transA2: all conformations populated when going from one basin to the other on the potential energy surface are thus taken into account in the calculation of the infrared spectrum. This population dynamics gives rise to a natural broadening of the calculated IR active bands, which is essential for the comparison to the experimental spectra.

(ii) When calculating IR spectra from the dipole time correlation function all anharmonic effects are naturally described. This is to be opposed to the two successive harmonic approximations usually adopted for the determination of IR spectra from static ab initio calculations (harmonic approximation of the potential energy surface at the optimized geometries and mechanical harmonic approximation for the transition dipole moments). Both approximations are released in ab initio molecular dynamics, simply because they are not needed. In fact, the finite temperature dynamics takes place on all accessible parts of the potential energy surface, be they harmonic or anharmonic. The quality of the potential energy surface is entirely contained in the "ab initio" force field, calculated at the DFT/BLYP level in this work. The good reproduction of the relative positions of the different active bands in this study is yet another demonstration that this level of theory is correct, as emphasized in our previous works on similar molecular systems.[33,34] Moreover, the calculation of IR spectra with molecular dynamics is related only to the time-dependent dipole moment of the molecule, and it does not require any harmonic expansion of the transition dipole moments. Therefore, if the dipole moments and their fluctuations are accurately calculated along the trajectory, the resulting IR spectrum should be reliable too, as demonstrated earlier.

As mentioned before, comparison of IR absorption intensities to the ones obtained in IR-MPD experiments is certainly not well understood. Equation 1 for the IR signal relies on linear response theory and is valid for one-photon linear-IR absorption spectroscopy. IR-MPD, on the other hand, is a multiphotonic IR absorption process leading to the fragmentation of the molecule. The recorded signal is the fragmentation yield with respect to each excitation IR wavelength. It is thus an indirect measurement of IR absorption in contrast to the usual linear-IR spectroscopy. Calculations and experiments are therefore not directly comparable for band intensities, giving rise to the observed discrepancies. The direct simulation of IR-MPD spectra, with a clear theoretical expression of the signal in terms of dynamical quantities, remains a totally open question.

Beyond protonated dialanine which can be considered as an interesting test case, the main purpose of the present work was to demonstrate the usefulness of finite temperature ab initio Car−Parrinello molecular dynamics simulations for the calculation of the infrared spectrum of complex flexible molecules in the gas phase, including larger peptides and biomolecules. This method goes beyond ab initio static calculations applied currently in the domain. Complex molecular systems display numerous energetically equivalent conformations which are difficult to be characterized with geometry optimization searches. Dynamics does release this difficulty. Moreover, the only ingredient needed for the calculation of IR spectra is the monitoring of the dipole moment at each time *t*.

We thus hope that our results open up a new door for the calculation, understanding, and interpretation of IR spectra of gas-phase molecules for which the conformational dynamics is fundamental. Note that only a few independent trajectories were needed in the present study to give a statistically meaningful IR spectrum. One can indeed anticipate an increase of the number of isomeric conformations accessible at room temperature for peptides composed of an increasing number of peptide units. In that case, an enhanced statistics will be required in order to capture the representative conformational dynamics. On the other hand, things may be simplified with larger peptides for which one can expect organized structures, such as helices or sheets, to be energetically predominant. Even in that case, however, structural coherent deformations may occur (in particular in the sub-1000 cm^{-1} frequency domain) which are to be sampled properly in order to relate to infrared spectra. That is where our molecular dynamics approach to complex molecules vibrational spectroscopy is going to.

Acknowledgment. The authors thank CINES (Montpellier, France) and IDRIS (Orsay, France) for generous access to their computational facilities. D.C.M. and M.P.G. acknowledge support from Genopole-France through the program 'ATIGE' Action Thématique Incitative de Génopole.

References and Notes

(1) Hillenkamp, F.; Karas, J.; Beavis, R. C.; Chait, B. T. *Anal. Chem.* **1991**, *63*, 1193A.

(2) Fenn, J. B.; Mann, M.; Meng, C. K.; Wong, S. F.; Whitehouse, C. M. *Mass Spectrom. Rev.* **1990**, *9*, 37.

(3) Smith, R. D.; Loo, J. A.; Edmonds, C. G.; Barinaga, C. J.; Udseth, H. R. *J. Am. Soc. Mass Spectrom.* **1990**, *62*, 882.
(4) Smith, R. D.; Loo, J. A.; Barinaga, C. J.; Edmonds, C. G.; Udseth, H. R. *J. Am. Soc. Mass Spectrom.* **1990**, *1*, 53.
(5) Krimm, S.; Bandekar, J. *Adv. Prot. Chem.* **1986**, *38*, 181.
(6) Torii, H.; Tasumi, M. *J. Chem. Phys.* **1992**, *96*, 3379.
(7) *Biological Applications of Raman Spectroscopy*; Spiro, T., Ed.; Wiley-Interscience: New York, 1987; Vol I.
(8) *Infrared Spectroscopy of Biomolecules*; Mantsch, H., Chapman, D., Eds.; Wiley-Liss: New York, 1996.
(9) Huang, R.; Kubelka, J.; Barber-Armstrong, W.; Silva, R. A. G. D.; Decatur, S. M.; Keiderling, T. A. *J. Am. Chem. Soc.* **2004**, *126*, 2346.
(10) Bour, P.; Keiderling, T. A. *J. Phys. Chem. B* **2005**, *109*, 5348.
(11) Oomens, J.; Meijer, G.; Helden, G. V. *J. Phys. Chem. A* **2001**, *105*, 8302.
(12) Lemaire, J.; Boissel, P.; Heninger, M.; Mauclaire, G.; Bellec, G.; Mestdagh, H.; Simon, A.; Le Caer, S.; Ortega, J. M.; Glotin, F.; Maitre, P. *Phys. Rev. Lett.* **2002**, *89*, 273002-1 and references therein.
(13) Kapota, C.; Ohanessian, G. *Phys. Chem. Chem. Phys.* **2005**, *7*, 3744.
(14) Kapota, C.; Lemaire, J.; Maitre, P.; Ohanessian, G. *J. Am. Chem. Soc.* **2004**, *126*, 1836.
(15) Lucas, B.; Gregoire, G.; Lemaire, J.; Maitre, P.; Ortega, J. M.; Rupenyan, A.; Reimann, B.; Schermann, J. P.; Desfrancois, C. *Phys. Chem. Chem. Phys.* **2004**, *6*, 2659.
(16) Lucas, B.; Gregoire, G.; Lemaire, J.; Maitre, P.; Glotin, F.; Schermann, J. P.; Desfrancois, C. *Int. J. Mass Spectrom.* **2005**, *243*, 105.
(17) Chin, W.; Piuzzi, F.; Dognon, J. P.; Dimicoli, I. L.; Tardivel, B.; Mons, M. *J. Am. Chem. Soc.* **2005**, *127*, 11900.
(18) Salpin, J. Y.; Guillaumont, S.; Tortajada, J.; MacAleese, L.; Lemaire, J.; Maitre, P. Manuscript in preparation.
(19) Kohtani, M.; Schneider, J. E.; Jones, T. C.; Jarrold, M. F. *J. Am. Chem. Soc.* **2004**, *126*, 16981.
(20) Wysocki, V. H.; Tsaprailis, G.; Smith, L. L.; Breci, L. A. *J. Mass. Spectrom.* **2000**, *35*, 1399.
(21) Paizs, B.; Csonka, I. P.; Lendvay, G.; Suhai, S. *Rapid Commun. Mass Spectrom.* **2001**, *15*, 637.
(22) Schlosser, A.; Lehmann, W. D. *J. Mass Spectrom.* **2000**, *35*, 1382.
(23) Johnson, R. S.; Martin, S. A.; Biemann, K. *Int. J. Mass Spectrom. Ion Processes* **1988**, *86*, 137.
(24) Cox, K. A.; Gaskell, S. J.; Morris, M.; Whiting, A. *J. Am. Soc. Mass Spectrom.* **1996**, *7*, 522.
(25) Zhang, K.; Zimmerman, D. M.; Chung-Philips, A.; Cassady, C. J. *J. Am. Chem. Soc.* **1993**, *115*, 10813.
(26) Campbell, S.; Rodgers, M. T.; Marzluff, E. M.; Beauchamp, J. L. *J. Am. Chem. Soc.* **1995**, *11*, 12840.
(27) Knapp-Mohammady, M.; Jalkanen, K. J.; Nardi, F.; Wade, R. C.; Suhai, S. *Chem. Phys.* **1999**, *240*, 63.
(28) Enriz, R. D.; Morales, M. E.; Baldoni, H. A. *J. Mol. Struct. (THEOCHEM)* **2005**, *731*, 177.
(29) Nandini, G.; Sathyanarayana, D. N. *J. Mol. Struct. (THEOCHEM)* **2003**, *638*, 79.
(30) Rodriguez, A. M.; Baldoni, H. A.; Suvire, F.; Vazquez, R. N.; Zamarbide, G.; Enriz, R. D.; Farkas, O.; Perczel, A.; McAllister, M. A.; Torday, L. L.; Papp, J. G.; Csizmadia, I. G. *J. Mol. Struct. (THEOCHEM)* **1998**, *455*, 275.
(31) Car, R.; Parrinello, M. *Phys. Rev. Lett.* **1985**, *55*, 2471.
(32) Marx, D.; Hutter, J. Ab initio molecular dynamics: theory and implementation. In *Modern methods and algorithms of quantum chemistry*; Grotendorst, J., Ed.; John von Meumann Institute for Computing: Julich, 2000; Vol. 1. NIC Series.
(33) Gaigeot, M.-P.; Sprik, M. *J. Phys. Chem. B* **2003**, *107*, 10344.
(34) Gaigeot, M.-P. Vuilleumier, R.; Sprik, M.; Borgis, D. *J. Chem. Theor. Comput.* **2005**, *1*, 772.
(35) Gaigeot, M.-P.; Sprik, M. *J. Phys. Chem. B* **2004**, *108*, 7458.
(36) Becke, A. *Phys. Rev. A* **1988**, *38*, 3098.
(37) Lee, C. Yang, W.; Parr, R. G. *Phys. Rev. B* **1988**, *37*, 785.
(38) Trouillier, N.; Martins, J. L. *Phys. Rev. B* **1991**, *43*, 1993.
(39) Kleinman, L.; Bylander, D. M. *Phys. Rev. Lett.* **1982**, *48*, 1425.
(40) Frisch, J. R.; Trucks, G. W.; Schlegel, H. B.; Scuseria, G. E.; Robb, M. A.; Cheeseman, J. R.; Zakrewski, V. G.; Montgomery, J. J. A.; Stratmann, R. E.; Burant, J. C.; Dapprich, S.; Milliam, J. M.; Daniels, A. D.; Kudin, K. N.; Strain, M. C.; Farkas, O.; Tomasi, J.; Barone, V.; Cossi, M.; Cammi, R.; Mennucci, B.; Pomelli, C.; Adamo, C.; Clifford, S.; Ochterski, J.; Petersson, G. A.; Ayala, P. Y.; Cui, Q.; Morokuma, K.; Malick, D. K.; Rabuck, A. D.; Raghavachari, K.; Foresman, J. B.; Cioslowski, J.; Ortiz, J. V.; Baboul, A. G.; Stefanov, B. B.; Liu, G.; Liashenko, A.; Piskorz, P.; Komaromi, I.; Gomperts, R.; Martins, R. L.; Fox, D. J.; Keith, T.; Allaham, M. A.; Peng, C. Y.; Nanayakkara, A.; Challacombe, M.; Gill, P. M. W.; Johnson, B.; Chen, W.; Wong, M. W.; Andres, J. L.; Gonzalez, C.; Head-Gordon, M.; Replogle, E.; Pople, J. A. *Gaussian 98*; Gaussian Inc.: Pittsburgh, PA, 1998.
(41) Martyna, G. J.; Tuckerman, M. E. *J. Chem. Phys.* **1999**, *110*, 2810.
(42) Hutter, J., et al. *CPMD, version 3.7.1*; IBM Research Division, IBM Corp and Max Planck Institute Stuttgart.
(43) McQuarrie, D. A. *Statistical Mechanics*; Harper-Collins Publishers: New York, 1976.
(44) Iftimie, R.; Tuckerman, M. E. *J. Chem. Phys.* **2005**, *122*, 214508.
(45) Borysow, J. Moraldi, M.; Frommhold, L. *Mol. Phys.* **1985**, *56*, 913.
(46) Ramirez, R.; Lopez-Ciudad, T.; Kumar, P.; Marx, D. *J. Chem. Phys.* **2004**, *121*, 3973.
(47) Silvestrelli, P. L.; Parrinello, M. *J. Chem. Phys.* **1999**, *111*, 3572.
(48) Silvestrelli, P. L.; Bernasconi, M.; Parrinello, M. *Chem. Phys. Lett.* **1997**, *277*, 478.
(49) Bernasconi, M.; Silvestrelli, P. L.; Parrinello, M. *Phys. Rev. Lett.* **1998**, *81*, 1235.
(50) Resta, R. *Phys. Rev. Lett*. **1998**, *80*, 1800.
(51) Vanderbilt, D.; King-Smith, R. D. *Phys. Rev. B* **1993**, *48*, 4442.
(52) Fischer, G. *Chem. Soc. Rev.* **2000**, *29*, 119.
(53) Mantz, Y. A.; Gerard, H.; Iftimie, R.; Martyna, G. J. *J. Am. Chem. Soc.* **2004**, *126*, 4080.